Exciton States in Free-Standing and Embedded Semiconductor Nanocrystals

Yuriel Núñez Fernández[1,2], Mikhail I. Vasilevskiy[1], Erick M. Larramendi[2] and Carlos Trallero-Giner[2,3]
[1]*Centro de Física, Universidade do Minho, 4710-057 Braga*
[2]*Facultad de Física and ICTM, Universidad de La Habana*
[3]*Departamento de Física, Universidade Federal de São Carlos*
[1]*Portugal*
[2]*Cuba*
[3]*Brazil*

1. Introduction

Semiconductor quantum dots (QDs), often referred to as "artificial atoms", have discrete energy levels that can be tuned by changing the QD size and shape. The existence of zero-dimensional states in QDs has been proved by high spectrally and spatially resolved photoluminescence (PL) studies Empedocles et al. (1996); Grundmann et al. (1995). Semiconductor QDs can be divided into two types, (1) epitaxially grown self-assembled dots (SAQDs) and (2) nanocrystals (NCs) surrounded by a non-semiconductor medium. Usually, SAQDs are obtained by using appropriate combinations of lattice mismatched semiconductors, taking advantage of the Stranski-Krastanov growth mode where highly strained 2D layers relax by forming 3D islands instead of generating misfit dislocations. SAQDs are robust and already integrated into a matrix appropriate for device applications Grundmann (2002). However, the size, shape and size distributions of the 3D islands are determined only by the strain related to the lattice mismatch of the specific heterojunction. Also, the density and the possibility of obtaining different nanocrystals over a given substrate have considerable limitations in this method.

Nanocrystal QDs have been produced by colloidal chemistry, melting, sputtering, ion implantation and some other techniques. An attractive feature of NCs is the possibility to control their electronic, optical and magnetic properties by varying their size, shape, surface characteristics and crystal structure, which is most efficiently achieved by using colloidal chemistry methods. These methods are known for the ability (i) to produce colloidal solutions of a broad variety of high quality semiconductor NCs of required size, (ii) to limit the size dispersion, and (iii) to control the NC surface Rogach (2008); Wang et al. (2005). Chemically grown NCs are more efficient light emitters than their bulk counterpart and even organic dyes. There are several reasons for this. First, quantum confinement of electronic states in QDs determines the transition energies and enhances the radiative transitions between conduction and valence bands. At the same time, it can be used to tune the luminescence wavelength and intensity, i.e., both the color and the brightness of the emission can be controlled. A second

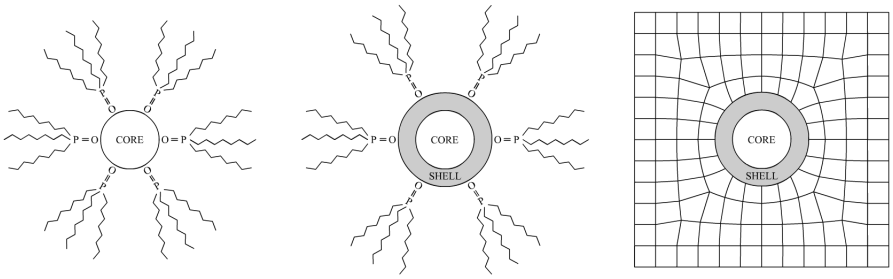

Fig. 1. Schematics of bare core (a) and core/shell (b) free standing and embedded (c) NC quantum dots.

effect, also characteristic of semiconductor nanoparticles, is not related to quantum physics but is purely geometrical. The spatial influence of defects acting as electronic traps is limited to the size of the host nanoparticle, whereas in bulk, nonradiative recombination sites can affect a much larger volume of material.

An obvious shortcoming of colloidal NCs, as compared to SAQDs, is that they are less stable and are not suitable for direct incorporation into electronic devices. One has to embed them into an appropriate matrix for device fabrication, especially for applications in the fields of optoelectronics and integrated optics. A possible approach consists in the integration of the colloidal chemistry methods with the epitaxial growth technology. The fabrication of high quality epitaxial films with embedded pre-fabricated NCs is a huge challenge. The successful integration of optically active colloidal NCs within an epitaxial structure has been demonstrated by combining the colloidal and molecular beam epitaxy (MBE) methods Woggon et al. (2005). It has been shown that core/shell nanoparticles (CSNPs) are more suitable for this purpose than bare core (e.g. CdSe) NCs. The luminescence properties and stability of CSNPs are generally better than those of single material nanocrystal QDs Rogach (2008). One of the earliest CSNP structures reported was CdSe/ZnS Dabbousi et al. (1997); Hines & Guyot-Sionnest (1996), which is at the same time the most intensively studied system to date. These particles show a very high photoluminescence (PL) quantum yield, which can be attributed to the better isolation of the electron-hole pair inside the dot from the surface recombination states. As well as NCs of a single semiconductor material, CSNPs are traditionally covered with trioctylphosphine oxide (TOPO) in order to prevent them from oxidation and to passivate dangling bonds at the semiconductor surface (See Fig. 1).

The nature of the medium surrounding a QD influences the quantum confinement effect and, consequently, the optical properties of these nanostructures. Already for colloidal NCs of a single II-VI material, the nature of the surface capping layer is important for the energy of the emitting states Jasieniak et al. (2011). For instance, exchange of TOPO with pyridine resulted in a a red shift of the order of 20-30 meV for CdSe NCs of 3.5-5.5 nm in diameter Luo et al. (2011). The transition energy and oscillator strength of the first excited state ($2S_{3/2}1S_e$) in these NCs can be strongly modified by their surface ligands and associated surface atomic arrangements Chen et al. (2011).

Introducing a shell also changes the energy spectrum of a colloidal QD. For CdSe/ZnS CSNPs, a red shift of the PL peak position and/or the absorption edge has been observed with

increasing the thickness of the ZnS shell Baranov et al. (2003); Dabbousi et al. (1997); Talapin et al. (2001). The value of the red shift usually saturates for the shell thicknesses (d_s) above 3 monolayers (MLs) Baranov et al. (2003); Talapin et al. (2001), which may be an indication of the typical length scale of core wavefunction's penetration into the shell. Quite interesting results indirectly confirming this idea have been obtained for ternary core/shell/shell structures with the outer shell of CdSe. For a thin (1-2 ML) ZnS inner shell, there is a red shift of the PL peak observed for increasing thickness of the outer shell (d_{ss}), while for d_s =3 ML the peak position is practically independent of d_{ss} Gaponik et al. (2010). It means that the tail of the wavefunction inside the barrier (the first shell) is smaller than 3ML. Finally, when NCs are embedded into an epitaxial semiconductor matrix, a *blue* shift of the PL peak is observed, compared to the emission spectrum of the same NCs in organic solvent Rashad et al. (2010); Woggon et al. (2005). This effect is not straightforward to explain, because, in a simple view, the replacement of TOPO by a semiconductor matrix with a band structure similar to that of the QD materials should result in lower barriers at the interface and, consequently, in a weaker confinement and a red shift of the exciton transition. Therefore, some further effects have to be included into consideration, such as interface imperfection, surface charge or strain introduced by the matrix.

The purpose of this chapter is to provide a general yet simple theoretical description of the effects of surrounding media (shells and matrix) and interface characteristics on the exciton ground state in nanocrystal QDs that would be able to explain the above mentioned experimental results and could be applied to more sophisticated semiconductor structures based on NCs of an approximately spherical shape. Our approach is based on the effective mass approximation (EMA). Its advantages and shortcomings for calculations of the electronic properties of nanostructures are well known. On one hand, it reveals the underlying physics and clearly shows the effect of the material parameters on the observable properties, this is why it has been used by so many research groups since the beginning of the studies of nanocrystal QDs in the 80-s Brus (1984); Efros et al. (1996); Fomin et al. (1998); Miranda et al. (2006); Norris & Bawendi (1996); Pellegrini et al. (2005); Rolo et al. (2008); Vasilevskii et al. (1998). On the other hand, EMA is believed to overestimate the electron and hole confinement energies Jasieniak et al. (2011). Also, the scaling laws of these energies with the QD radius (R), obtained by fitting experimental Yu et al. (2003) and numerically calculated Delerue & Lannoo (2004) data, differ from the EMA predictions (R^{-2} in the strong confinement regime). Indeed, the EMA fails in the limit of very small clusters containing a hundred of atoms which should not even be called nanocrystals because their properties have more similarity with molecules than with crystals. Compared to the first version of the EMA theory for QDs Brus (1984), several improvements have been made, such as the consideration of finite barriers Norris & Bawendi (1996); Pellegrini et al. (2005) and the complex structure of the valence band of the underlying material Efros et al. (1996). As a result, it has been possible to assign several size-dependent transitions in measured optical spectra of CdSe Norris & Bawendi (1996) and CdTe Vasilevskii et al. (1998) QDs. Further improvement of the analytical description of QDs can be achieved by considering generalized boundary conditions allowing a discontinuity of the envelope functions at the interfaces, found to provide a better agreement with the results of *ab initio* numerical calculations Flory et al. (2008).

We apply the EMA approach to arbitrary centrosymmetric potentials, such as finite interface barriers due to band discontinuities or electric charges that can eventually accumulate at the NC/matrix interface. The EMA equations for electrons and holes (taking into account the

complex valence band structure) will be formulated in terms of transfer matrices, allowing for the incorporation of generalized boundary conditions at all interfaces. The resulting matrix equations are solved numerically providing a rather simple and efficient tool for modeling different experimental situations and designing new complex QD-based nanostructures and optoelectronic devices with embedded nanoparticles as active optical components. The developed open-source software is available at http://sourceforge.net/projects/emaqdot. Finally, we present some calculated results concerning free-standing and embedded QDs and check them against experimental trends reported in the literature.

2. Exciton transition energy calculation

2.1 Basic equations

In the strong confinement regime ($R \ll a_{ex}$, a_{ex} is the exciton Bohr radius, and R is the core radius), the calculation of the lowest ($1S_{3/2}1S_e$) transition energy requires the electron ground state energy, E_e, the hole ground state energy, E_h, and the Coulomb interaction correction, E_c,

$$E_t = E_g + E_e + E_h + E_c$$

where E_g is the band gap energy of the core material. $E_e(E_h)$ is defined with respect to the bottom (top) of the conduction (valence) band.

For the spherically symmetric electron state $1S_e$, the envelope wavefunction can be written as $\Psi_e = \psi(r)/\sqrt{4\pi}r$ and the effective Schrï£¡dinger equation for $\psi(r)$ reads Efros et al. (1996); Norris & Bawendi (1996); Vasilevskii et al. (1998):

$$\psi''(r) + \frac{2m_e}{\hbar^2}\left[E_e - V_e(r)\right]\psi(r) = 0, \tag{1}$$

where m_e is the electron effective mass and $V_e(r)$ is the potential acting on the electron. In order to obtain the electron ground state energy, we have to solve Eq. (1) together with the boundary conditions $\psi(0) = \psi(\infty) = 0$ and a matching condition at each interface of the heterostructure (see below).

Owing to the complex valence band structure of the involved semiconductor materials, the hole ground state is determined by the Luttinger Hamiltonian Luttinger (1956). In the centrosymmetric case, the radial part of the wavefunction is determined by two functions, $R_0(r)$ and $R_2(r)$, which satisfy the following system of differential equations Gelmont & Diakonov (1972):

$$(1+\beta)\left(\frac{d}{dr}+\frac{2}{r}\right)\frac{dR_0}{dr} + (1-\beta)\left(\frac{d}{dr}+\frac{2}{r}\right)\left(\frac{d}{dr}+\frac{3}{r}\right)R_2 + 4\frac{m_{lh}}{\hbar^2}\left(E_h - V_h(r)\right)R_0 = 0 \tag{2}$$

$$(1-\beta)\left(\frac{d}{dr}-\frac{1}{r}\right)\frac{dR_0}{dr} + (1+\beta)\left(\frac{d}{dr}-\frac{1}{r}\right)\left(\frac{d}{dr}+\frac{3}{r}\right)R_2 + 4\frac{m_{lh}}{\hbar^2}\left(E_h - V_h(r)\right)R_2 = 0 \tag{3}$$

where $V_h(r)$ is the potential acting on the hole,

$$\beta = \frac{\gamma_1 - 2\gamma}{\gamma_1 + 2\gamma} = \frac{m_{lh}}{m_{hh}}$$

and

$$m_{lh} = \frac{m_0}{\gamma_1 + 2\gamma}, \qquad m_{hh} = \frac{m_0}{\gamma_1 - 2\gamma}$$

are the light and heavy holes masses, respectively. Here, m_0 is the free electron mass and γ_1 and γ=$(2\gamma_2 + 3\gamma_3)$ /5 are the Luttinger parameters. They are constant within each material.

Finally, the Coulomb interaction energy is given by

$$E_c = -\frac{e^2 C}{\epsilon R} \tag{4}$$

where ϵ is the static dielectric constant of the QD material [1] and

$$C = \int_0^\infty t^2 \left[R_0^2(t) + R_2^2(t)\right] \left\{ \frac{1}{t} \int_0^t \psi^2(s) ds + \int_t^\infty \frac{\psi^2(s)}{s} ds \right\} dt,$$

assuming that ψ, R_0 and R_2 are normalized according to:

$$\int_0^\infty \psi^2(t) dt = 1,$$

$$\int_0^\infty \left[R_0^2(t) + R_2^2(t)\right] t^2 dt = 1.$$

2.2 Boundary conditions

The differential equations presented above hold only inside each (e.g. core) material. At an interface between two materials, the following continuity conditions for the electron wavefunction should be applied:

$$\Psi_e \text{ and } \frac{1}{m_e} \frac{d\Psi_e}{dr} \text{ continuous.} \tag{5}$$

However, as it has been mentioned in the Introduction, the wavefunction $\psi(r)$ is just an *envelope* function and not necessarily must be continuous Flory et al. (2008); Laikhtman (1992). This issue has been widely discussed in the literature in relation to semiconductor heterostructures (see references in Laikhtman (1992)). Instead of (5), more general boundary conditions have been proposed, providing a better agreement with *ab initio* calculations for a number of III-V and II-VI compound heterostructures. A simplified version of such generalized boundary conditions that guarantees the continuity of the probability flux reads Rodina et al. (2002):

$$(m_e)^\alpha \Psi_e \quad \text{and} \quad \frac{1}{(m_e)^{\alpha+1}} \frac{d\Psi_e}{dr} \text{ continuous.} \tag{6}$$

where α is a phenomenological parameter. We shall also use these conditions (5) for interfaces between a semiconductor and TOPO. For $\alpha = 0$ the wavefunction is continuous while for $\alpha \neq 0$ it is not because of the difference in effective masses m_e at the interface.

At an ideal interface of two semiconductor materials of the same symmetry, the following continuity conditions for the hole envelope functions take place:

$$\begin{aligned} R_0,\ R_2 &\text{ continuous;} \\ \frac{1}{m_{lh}} \frac{d}{dr} \left(R_0 + R_2\right) &\text{ continuous;} \\ \frac{1}{m_{hh}} \frac{d}{dr} \left(R_0 - R_2\right) &\text{ continuous.} \end{aligned} \tag{7}$$

[1] For simplicity, we neglect the difference in the dielectric constant between different materials.

Although, in principle, these conditions should also be replaced by generalized ones, similar to Eqs. (6) Laikhtman (1992), we preferred to keep (7) in order to avoid additional free parameters.

2.3 Solution via transfer matrices

Since the equations are one-dimensional and the boundary conditions are linear, a transfer matrix formalism can be applied. This approach, borrowed from the optics of multilayer media Born & Wolf (1989), offers a convenient framework for linear problems and is straightforward to implement in a computer.If the potentials $V_e(r)$ and $V_h(r)$ are constant inside each material, Eqs. (1 - 3) can be solved explicitly. Considering one such material, two linearly independent solutions of (1) are $\cos(k_e r)$ and $\sin(k_e r)$ if

$$k_e = \sqrt{\frac{2m_e}{\hbar^2}\left(E_e - V_e\right)}$$

is real. If it is imaginary, $k_e = i\kappa_e$, then the solutions are $\exp(\pm\kappa_e r)$. For holes, if

$$k_h = \sqrt{\frac{2m_{hh}}{\hbar^2}\left(E_h - V_h\right)}$$

is real, the linearly independent solutions of Eqs. (2, 3) for the 2-vector $\begin{pmatrix} R_0 \\ R_2 \end{pmatrix}$ are

$$\begin{pmatrix} j_0(k_h r) \\ j_2(k_h r) \end{pmatrix}, \begin{pmatrix} j_0(k_l r) \\ -j_2(k_l r) \end{pmatrix}, \begin{pmatrix} y_0(k_h r) \\ y_2(k_h r) \end{pmatrix}, \begin{pmatrix} y_0(k_l r) \\ -y_2(k_l r) \end{pmatrix}, \tag{8}$$

where $k_l = \sqrt{\beta}k_h$, and j_ν, y_ν are the spherical Bessel functions of the first and second kind, respectively.

If $k_h = i\kappa_h$ with κ_h real, the solutions are:

$$\begin{pmatrix} i_0(\kappa_h r) \\ -i_2(\kappa_h r) \end{pmatrix}, \begin{pmatrix} i_0(\kappa_l r) \\ i_2(\kappa_l r) \end{pmatrix}, \begin{pmatrix} k_0(\kappa_h r) \\ -k_2(\kappa_h r) \end{pmatrix}, \begin{pmatrix} k_0(\kappa_l r) \\ k_2(\kappa_l r) \end{pmatrix}, \tag{9}$$

where $\kappa_l = \sqrt{\beta}\kappa_h$, and $i_\nu(z)$, $k_\nu(z)$ are the modified spherical Bessel functions of the first and third kind, respectively Abramowitz & Stegun (1970). Collecting the above solutions and combining them by using the boundary and matching conditions, one can obtain some transcendental equations for E_e and E_h. These transcendental equations are conveniently expressed in terms of transfer matrices, as shown below. For general centrosymmetric potentials, $V_e(r)$ and $V_h(r)$, the solutions of Eqs. (1-3) inside each material cannot be found analytically. The differential equations must be discretized using an appropriate numerical scheme. Then, our general approach still remains valid.

Let us suppose that $V_e(r)$, $V_h(r) = \text{const}$ in the following regions of the heterostructure: $0 < r < A_1$ (core) and $r > A_N$ (matrix far from the NC interface). Then the solutions in these regions are given by some particular combination of the above expressions (8) or (9). We consider a 2-vector, composed of the electron wavefunction and its derivative, $\mathbf{z}_e(r) = \begin{pmatrix} \psi(r) \\ \psi'(r) \end{pmatrix}$, which can be written explicitly for $r = A_1$ and $r = A_N$. These two vectors are

connected by a transfer matrix, $\mathbf{T}_e$, that characterizes the region $r \in [A_1, A_N]$. It is constructed by multiplying the elementary transfer matrices describing the layers $A_i \leq r \leq A_{i+1}$, $(i = 2, 3, ..., N-1)$, and their interfaces. The details are given in Appendix I for a constant potential profile and in Appendix II for an arbitrary potential. Note that the case of infinite potential barrier at A_N requires a special analysis and is considered in Appendix III. Explicitly, we have for $r = A_1$:

$$\mathbf{z}_e(A_1) = c_1 \mathbf{v}_1$$

where

$$\mathbf{v}_1 = \begin{pmatrix} \sin(k_e A_1) \\ k_e \cos(k_e A_1) \end{pmatrix} \qquad (E_e > V_e),$$

or

$$\mathbf{v}_1 = \begin{pmatrix} \sinh(\kappa_e A_1) \\ \kappa_e \cosh(\kappa_e A_1) \end{pmatrix} \qquad (E_e < V_e).$$

For $r = A_N$,

$$\mathbf{z}_e(A_N) = c_2 \mathbf{v}_2 \qquad (E_e < V_e),$$

$$\mathbf{v}_2 = \begin{pmatrix} \exp(-k_e A_N) \\ -k_e \exp(-k_e A_N) \end{pmatrix}.$$

Connecting the points A_1 and A_N, we get

$$c_2 \mathbf{v}_2 - c_1 \mathbf{v}_3 = \mathbf{0}, \tag{10}$$

$$\mathbf{v}_3 = \mathbf{T}(A_1, A_N) \cdot \mathbf{v}_1.$$

The energy E_e is obtained from the equation,

$$\det\left(\left[\, -\mathbf{v}_3 \; \mathbf{v}_2 \,\right]\right) = 0. \tag{11}$$

Similarly, the corresponding 4-vectors for holes composed of $\begin{pmatrix} R_0 \\ R_2 \end{pmatrix}$ and their derivatives, are connected by a 4×4 transfer matrix $\mathbf{T}_h$ (see Appendix I). For $r = A_1$, we have:

$$\mathbf{z}_h(A_1) = c_1 \mathbf{v}_1 + c_2 \mathbf{v}_2,$$

where

$$\mathbf{v}_1 = \begin{pmatrix} j_0(k_h A_1) \\ j_2(k_h A_1) \\ k_h j_0'(k_h A_1) \\ k_h j_2'(k_h A_1) \end{pmatrix}, \mathbf{v}_2 = \begin{pmatrix} j_0(k_l A_1) \\ -j_2(k_l A_1) \\ k_l j_0'(k_l A_1) \\ -k_l j_2'(k_l A_1) \end{pmatrix} \qquad (E_h > V_h)$$

or

$$\mathbf{v}_1 = \begin{pmatrix} i_0(\kappa_h A_1) \\ -i_2(\kappa_h A_1) \\ \kappa_h i_0'(\kappa_h A_1) \\ -\kappa_h i_2'(\kappa_h A_1) \end{pmatrix}, \mathbf{v}_2 = \begin{pmatrix} i_0(\kappa_l A_1) \\ i_2(\kappa_l A_1) \\ \kappa_l i_0'(\kappa_l A_1) \\ \kappa_l i_2'(\kappa_l A_1) \end{pmatrix} \qquad (E_h < V_h).$$

For $r = A_N$,

$$\mathbf{z}_h(A_N) = c_3 \mathbf{v}_3 + c_4 \mathbf{v}_4$$

where

$$\mathbf{v}_3 = \begin{pmatrix} k_0(\kappa_h A_N) \\ -k_2(\kappa_h A_N) \\ \kappa_h k_0'(\kappa_h A_N) \\ -\kappa_h k_2'(\kappa_h A_N) \end{pmatrix}, \mathbf{v}_4 = \begin{pmatrix} k_0(\kappa_l A_N) \\ k_2(\kappa_l A_N) \\ \kappa_l k_0'(\kappa_l A_N) \\ \kappa_l k_2'(\kappa_l A_N) \end{pmatrix} \qquad (E_h < V_h).$$

Connecting the points $r = A_1$ and $r = A_N$, we have

$$c_3\mathbf{v}_3 + c_4\mathbf{v}_4 - c_1\mathbf{v}_5 - c_2\mathbf{v}_6 = \mathbf{0}, \tag{12}$$

$$\mathbf{v}_5 = \mathbf{T}_h(A_1, A_N)\cdot\mathbf{v}_1, \qquad \mathbf{v}_6 = \mathbf{T}_h(A_1, A_N)\cdot\mathbf{v}_2.$$

The energy E_h is determined by the equation

$$\det\left(\left[-\mathbf{v}_5\ -\mathbf{v}_6\ \mathbf{v}_3\ \mathbf{v}_4\right]\right) = 0. \tag{13}$$

2.4 Too low barrier for holes

For embedded QDs, it is quite possible that the potential barriers provided by the semiconductor matrix are not sufficiently high (because of the small valence band-offset for II-VI semiconductors) to confine the carriers if the core radius is very small. Then one cannot consider the Coulomb interaction as a perturbation anymore and the confinement of the exciton as a whole should be considered. However, it can happen that the conduction band barrier is still quite high and the electrons still are in the strong confinement regime (i. e., $R \ll a_e$, a_e is the electron Bohr radius for the core material). Then the Coulomb interaction with the hole is still a small perturbation for the electron. Its ground state energy E_e and the wavefunction $\Psi_e(r)$ can be found as before. The above condition has profound physical consequences. The strongly localized electron shall keep the hole in the vicinity of the dot (otherwise it would be free to move into the matrix). This case can be called as "weak localization of the hole". We shall extend our formalism in order to include this case.

The Schrï£¡dinger equation for the electron-hole pair (exciton) is written as

$$\left[\hat{T}_e + V_e(\mathbf{r}_e) + \hat{T}_h + V_h(\mathbf{r}_h) + V_{eh}(\mathbf{r}_e, \mathbf{r}_h)\right]\psi_{eh} = E_{ex}\Psi_{ex}$$

where $\Psi_{ex} = \Psi_e(\mathbf{r}_e)\Psi_h(\mathbf{r}_h)$ (Ψ_h is a 2-vector), $\hat{T}_e$ ($\hat{T}_h$) represents the electron (hole) kinetic energy operator and V_{eh} is the electron-hole Coulomb interaction term. Multiplying by Ψ_e^* and integrating over the electron coordinates, $\mathbf{r}_e$, yields:

$$\left[\hat{T}_h + V_h(\mathbf{r}_h) + V_{\text{eff}}(\mathbf{r}_h)\right]\Psi_h = E_h\Psi_h \tag{14}$$

with

$$V_{\text{eff}} = \langle\Psi_e\,|V_{eh}|\,\Psi_e\rangle\,.$$

Using the well-known expansion,

$$\frac{1}{|\mathbf{r}_e - \mathbf{r}_h|} = \begin{cases} \frac{1}{r_e}\sum_{l=0}^{\infty}\left(\frac{r_h}{r_e}\right)^l P_l(\cos\theta) & \text{if } r_e \geq r_h \\ \frac{1}{r_h}\sum_{l=0}^{\infty}\left(\frac{r_e}{r_h}\right)^l P_l(\cos\theta) & \text{if } r_e < r_h \end{cases},$$

where P_l are Legendre polynomials and $\Psi_e(\mathbf{r}_e) = \psi(r_e)/\sqrt{4\pi}r_e$, we have:

$$V_{\text{eff}}(r_h) = -\frac{e^2}{\epsilon r_h}\int_0^{r_h}\psi^2(r_e)dr_e - \frac{e^2}{\epsilon}\int_{r_h}^{\infty}\frac{1}{r_e}\psi^2(r_e)dr_e. \tag{15}$$

For large r_h, the probability to find the electron there is small and $V_{\text{eff}}(r_h)$ behaves as $-e^2/\epsilon r_h$. On the other hand, for small r_h we have $V_{\text{eff}}(r_h) = V_{\text{eff}}(0) + O(r_h^2)$, where

$$V_{\text{eff}}(0) = -\frac{e^2c_1^2}{2\epsilon}\left[\Gamma - Ci(2k_eR) + \ln(2k_eR)\right] - \frac{e^2}{\epsilon}\int_R^{\infty}\frac{\psi^2(r)}{r}dr,$$

Γ is the Euler-Mascheroni constant, $C_i(x)$ is the cos-integral function, and k_e, c_1 are the electron parameters inside the core (see above). Figure 2 shows the shape of the effective potential $V_{\text{eff}}(r_h)$.

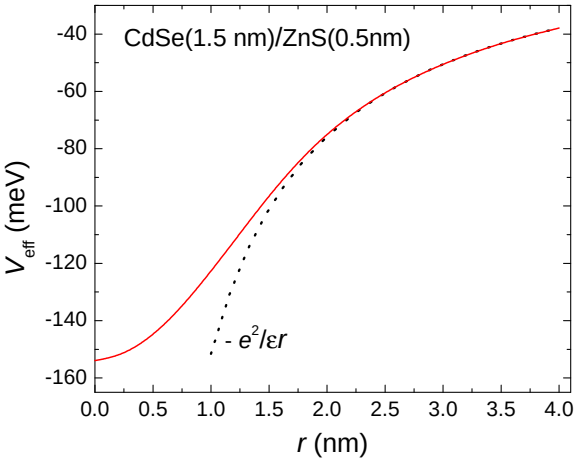

Fig. 2. Effective potential for holes (Eq. 15) produced by localized electron in $1S_e$ state.

This potential has to be added to V_h in Eqs. (2) and (3). Because of the non-explicit expression (15) for V_{eff} we have to solve (14) numerically. However, this does not rise any difficulty because this potential is also centrosymmetric (Appendix II). The asymptotic solutions for both $r_h \to 0$ and $r_h \to \infty$ are required. Near the origin, the potential $V_{\text{eff}}(r_h)$ is almost constant and the above mentioned solutions, $\mathbf{v}_1$ and $\mathbf{v}_2$, can be used (by putting $V_{\text{eff}}(r_h) \approx V_{\text{eff}}(0)$). In the same way, for large r_h the dominating terms of the asymptotic solutions behave as $\mathbf{v}_3$, $\mathbf{v}_4$ (replacing $V_{\text{eff}}(r_h)$ by 0).

Applying the continuity conditions similar to (7) and using the numerical transfer matrices described in Appendix II, the solutions of Eq. (14) near $r_h = 0$ are connected with the asymptotic ones at $r_h = A_N$, and the energy E_h is obtained.

3. Results and discussion

We applied the formalism described in the previous section to a set of "samples" that mimic free standing and embedded bare core and core/shell NCs. The parameters used in the calculations are listed in Table 1. The results are summarized below.

Bare core NCs

Concerning the size-dependent lowest transition energy in bare core NCs covered by TOPO Fig. 3 shows the results of our calculations in comparison with the experimental data of Murray et al. (1993); Yu et al. (2003) and those calculated assuming infinitely high barriers. A good agreement with the experiment is observed only for the calculations performed with finite barriers Pellegrini et al. (2005). We would like to point out that the complex valence band structure was neglected in the previous work considering finite barriers Pellegrini et al. (2005) and, consequently, an unrealistically small effective mass ($0.3m_0$) for heavy holes was

Parameter	$CdSe$	ZnS	$ZnSe$	$TOPO$
$m_e(m_0)$	0.119	0.22	0.16	1
$m_{hh}(m_0)$	0.82	0.61	0.495	1
$m_{lh}(m_0)$	0.262	0.23	0.177	1
E_g(eV)	1.75	3.78	2.7	5
VBO(eV)	0	0.99	0.22	1.63

Table 1. Parameters used in calculations for CdSe, ZnS, and ZnSe. Notation: VBO , E_g, m_e, m_{hh} and m_{lh} refer to the valence band offset, band gap, and effective masses of electrons, heavy holes and light holes, respectively. These values were taken from Li et al. (2009); Pellegrini et al. (2005); Schulz & Czycholl (2005); *Springer Materials The Landolt-Börnstein Database* (2011).

used. In the present work, we used the correct model for the valence band with realistic m_{lh} and m_{hh} and introduced an extra parameter $\alpha_{CdSe/TOPO} = -0.08$ to characterize the electron envelope function matching at the CdSe/TOPO interface. Barrier's heights used by Pellegrini et al. (2005) (1.63 eV) were obtained by subtracting semiconductor's E_g from the known energy (5 eV) of a certain electronic transition in TOPO and dividing the result equally between the CB and VB offsets, yielding the above rather low values. Most of the authors used much higher values for these barriers Dabbousi et al. (1997); Rashad et al. (2010) in order to obtain the correct trends for core-shell structures (see below) but then it is not possible to correctly reproduce the $E_t(R)$ dependence for bare core particles. Using the discontinuous envelope function can help to remedy this difficulty.

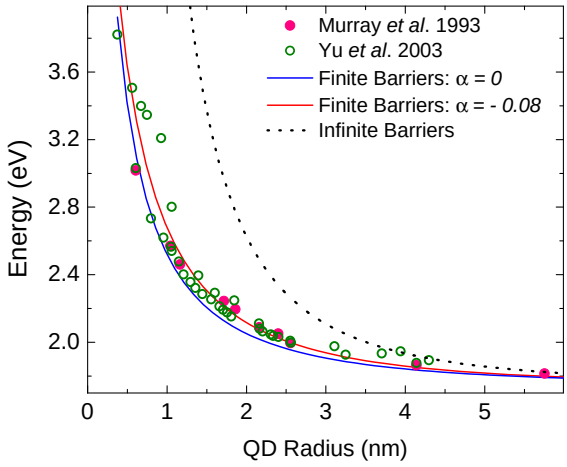

Fig. 3. Comparison between experimental and theoretical results for CdSe/TOPO NCs. Experimental values were taken from Refs. Murray et al. (1993); Yu et al. (2003). The lowest transition energy was calculated using finite barriers and either continuous ($\alpha = 0$) or discontinuous ($\alpha \neq 0$) boundary conditions for the electron wavefunction at the interface. For comparison, the results obtained assuming infinitely high barriers for both electron and hole are also presented.

Shell thickness effect in CdSe/ZnS CSNCs

As it has been said in the Introduction, the absorption and PL emission peaks in the spectra of CdSe/ZnS core/shell NCs are redshifted with respect to the bare core CdSe NCs of the same radius. The shift grows when the shell thickness is increased up to d_s=3 ML and then saturates. This effect has been observed by several groups Baranov et al. (2003); Dabbousi et al. (1997); Soni (2010). We focus on the absorption peak position because the emission peak is usually Stokes-shifted with respect to the former mostly because of the size distribution effects (larger dots emit stronger than the smaller ones in an ensemble of NCs Efros et al. (1996)). In our calculations of the lowest transition energy, the electron wavefunction at the CdSe/ZnS interface was considered continuous ($\alpha = 0$), while the ZnS/TOPO interface was characterized by an appropriate (non-zero) value of the electron wavefunction discontinuity parameter, $\alpha_{ZnS/TOPO}$. Fig. 4 shows a good agreement between the calculated and experimental results, obtained without using an unrealistically large heights of the ZnS/TOPO barriers (like 10 eV for holes in Ref. Dabbousi et al. (1997)). For comparison, the case $\alpha_{ZnS/TOPO} = 0$ is also presented, which lead to a blue shift in the transition energy when the shell thickness is increased, in direct contradiction with the experiments.

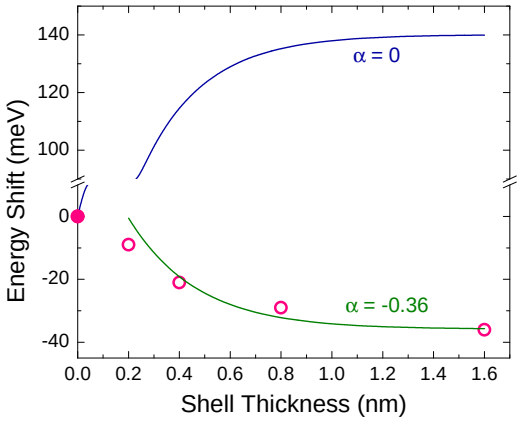

Fig. 4. Absorption peak shift in CdSe/ZnS CSNC, obtained experimentally by Dabboussi *et al.* (points) and calculated using present model with $\alpha_{ZnS/TOPO} = -0.36$ and $\alpha_{ZnS/TOPO} = 0$. The transition energy for the core/shell NCs is measured with respect to the CdSe bare core QD. The core size in both cases is $R = 2.0$ nm.

The effect of surface charge

As it has been pointed out in the Introduction, the utilization of colloidal NCs as active optical material in optoelectronic devices requires their incorporation into a high quality solid matrix. This process comprises the casting of the colloidal particles onto a substrate with the subsequent overgrowth of the matrix. For such embedded structures, it is relevant to consider the possibility of static charge accumulation at the nanoparticle/matrix interface Baccarani et al. (1978). Because of the incoherent incorporation of the nanoparticles into the crystalline matrix, the interface can create electronic trap states. Therefore the surface should be charged

with a density σ_0 and a compensating space charge should be distributed in the matrix in the vicinity of the particle. The volume density of the latter can be assumed of the form,

$$\rho_m(r) = -\rho_0 \exp\left[-\frac{r-r_0}{l}\right] \qquad (r > r_0), \tag{16}$$

where $r_0 = R + d_s$ is the radius of the particle, l is a characteristic length (of the order of 1-2 nm), and ρ_0 is obtained from the charge neutrality condition:

$$\rho_0 = \frac{\sigma_0}{l\left[1 + 2l/r_0 + 2\left(l/r_0\right)^2\right]}.$$

Since epitaxial ZnSe normally is intrinsically n-type doped, we assume $\sigma_0 < 0$.

The electrostatic potential, $\varphi(r)$, is found by solving the Poisson equation with the charge density $\rho(r) = \sigma_0\delta(r - r_0) + \rho_m(r)$. The additional potential energy is:

$$U_c(r) = -e\varphi(r) = \begin{cases} AU_0 \frac{2l/r+1}{2l/r_0+1} \exp\left[-\frac{r-r_0}{l}\right] & (r \geq r_0) \\ AU_0 & (r < r_0) \end{cases}, \tag{17}$$

where $A = \left(l/r_0\right)\left(2l/r_0 + 1\right)\left[1 + 2l/r_0 + 2\left(l/r_0\right)^2\right]^{-1}$ is a dimensionless constant and the energy $U_0 = -4\pi r_0\sigma_0 e/\epsilon$. Then the confinement potentials for electron and hole are obtained by considering $U_c(r)$ and the conduction and valence band offsets between the different materials forming each structure. The resulting band diagrams for two heterostructures (for the case of $\sigma_0 < 0$) are shown in Figure 5 a, b. Notice that, according to (17), if $l \ll r_0$ then the electron confinement decreases while the hole wavefunction becomes stronger localized owing to the surface charge effect. For large l the surface charge effect on the confinement can be neglected.

The results obtained for CdSe and CdSe/ZnS nanoparticles embedded in ZnSe are presented in Figs. 5-c, and 5-d. It can be seen that the surface charge effect on the hole energy is stronger for the bare core QD than for the CSNP. This is because in the latter, because of the presence of the ZnS shell, the hole penetrates less into the matrix (see Fig. 5 a, b) and hence a weaker interaccion with the charged interface is expected [2]. As a result, the surface charge effects on the electron and the hole nearly compensate each other in a bare core NC, while in a core/shell QD there is a significant net red shift of the exciton transition owing to the presence of the surface charge.

Free-standing *versus* embedded NCs

A blue shift in the PL emission when CdSe/ZnS CSNCs were embedded into a ZnSe crystalline matrix was observed in the work Larramendi (n.d.). Two samples studied in that work contained nanocrystals with different core size, $2R = 2.5$ and 3.0 nm, and $d_s = 0.5$ nm of ZnSe shell (2 MLs). A shift of the emission peak, of 68 and 33 meV, respectively, was observed (Fig. 6). We attempted to reproduce this effect in our calculations. Here we used $\alpha = 0$ for all (CdSe/ZnS, ZnS/TOPO, and ZnS/ZnSe) interfaces.

[2] For $r < R$ the hole does not interact with the charges outside by virtue of the Gauss law.

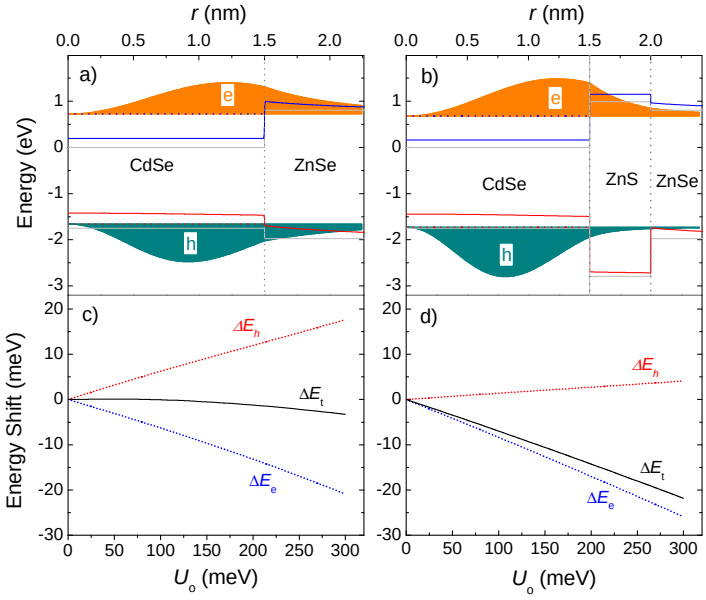

Fig. 5. Band energy diagrams for CdSe/ZnSe (a) and CdSe/ZnS/ZnSe (b) structures, with (full lines) and without (dashed lines) charge at the NC/matrix interface. Notice that the valence and conduction bands are shifted by a constant value (equal to AU_0) inside the particle. Also shown are the electron and hole probability densities for the case with surface charge. In panels c) and d) the electron (blue), the hole (red), and the transition (black) energy shifts (with respect to the case of $\sigma_0 = 0$) are presented *versus* the surface charge parameter U_0.

The results of our calculations are presented in Fig. 6. Essentially, the blue shift is obtained in a natural way, despite the higher barrier for TOPO-covered free-standing NCs. In order to qualitatively understand this result, we focus on Fig. 7, particularly on the electron wavefunctions shown in Fig. 7 d, which exemplifies the situation. For the free-standing NC, the higher barrier results in a smaller penetration length. This would favor larger energies. However, the larger difference in the effective masses on the left and on the right of the interface implies an abrupt change in the slope of the wavefunction. For the given set of parameters, the second effect (i.e. the change in the derivative of Ψ_e at the interface) dominates. Despite the longer tail of the electron wavefunction in the case of the embedded QD, the maximum of the probability density is located at a lower distance from the center and a blue shift is obtained (except for the smallest radii).

Let us point out that the situation depicted in the right panels of Fig. 7 corresponds to weak localization of the hole owing to its the Coulomb interaction with the strongly localized electron. Passing from strong to weak localization should affect the overlap integral between the electron and hole wavefunctions that determines the transition oscillator strength. In the ultimate limit of small core radius, the electron becomes delocalized and, consequently, the hole too. Then the overlap integral should decrease drastically. It could explain why the luminescence of the bare core NCs is weaker than that of the core shell NCs when they

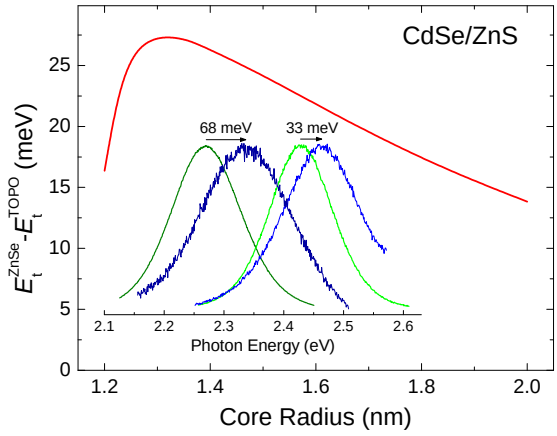

Fig. 6. Calculated transition energy shift *versus* core radius for CdSe/ZnS CSNPs embedded in ZnSe matrix ($d_s = 0.5$nm, $\sigma_0 = 0$). In the inset are displayed the PL bands measured for two samples of colloidal CdSe/ZnS NCs with different core size (2.5 and 3.0 nm), dispersed in toluene solution (green lines) and after embedding into epitaxial ZnSe layer (blue lines) [courtesy of Prof. U. Woggon and Dr. O. Schï£¡ps].

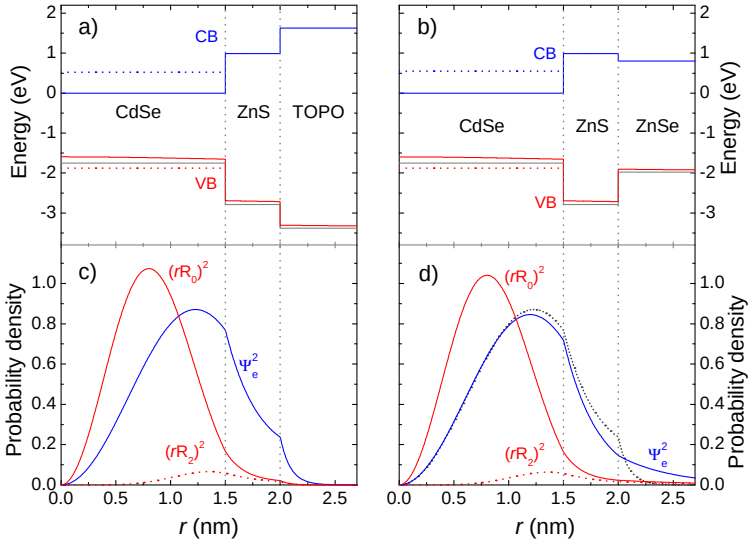

Fig. 7. Potential profiles and probability densities [electron (blue), $(rR_0)^2$ (red solid) and $(rR_2)^2$ (red dashed)] for CdSe/ZnS/TOPO nanoparticle (left panels) and CdSe/ZnS/ZnSe heterostructure (right panels). In the latter, the electron density of panel c) is also shown for comparison (black dotted line). In both cases $R = 1.5$ nm, $d_s = 0.5$ nm, $\sigma_0 = 0$, and $\alpha = 0$.

are embedded into the matrix Larramendi (n.d.). The threshold (in terms of the core size) between the different confinement regimes depends on several factors, such as the band

offsets. These can be affected by the electric charge that can accumulate at the interface between the embedded QDs and the matrix. For instance, a positive surface charge would increase the electron barrier and decrease the one for the hole. The charge would also modify the potential profile seen by the confined electrons and holes, similar to the effect known for polycrystalline silicon Baccarani et al. (1978). It could bring about the hole confinement in the vicinity of the CdSe/ZnS interface, similar to what happens to 2D electrons in AlGaAs/GaAs heterostructures.

4. Conclusions

In summary, we have developed a transfer matrix approach to theoretically describe the effects of surrounding media and interface charge on the exciton ground state in nanocrystal QDs. It permits to explain a number of experimentally observed effects, including (i) the size-dependent lowest transition energy, (ii) the influence of shell thickness on the absorption and emission spectra of core/shell nanoparticles and (iii) the blue shift of the emission peak when NCs are embedded into an epitaxial matrix. For this, the utilization of generalized boundary conditions at nanoparticle/organic-ligand interfaces is required. We also showed that the Coulomb interaction between the electron and the hole can be important for the confinement of the latter. This is essential for the interpretation of the experimental results concerning colloidal CdSe NCs embedded in a semiconductor (e.g. ZnSe) host matrix because of the small valence band-offset between II-VI semiconductors. Note that, since the colloidal NCs are buried with random crystalline orientations and, consequently, are non-coherent to the host epitaxial matrix, the influence of the strain that could result from the lattice mismatch between the NCs and the matrix is not expected and therefore was not taken into account in our model. However, it could be incorporated using the standard theory of strained bulk semiconductors Bir & Pikus (1974). The same applies to the effects of the electron-hole exchange interaction and crystal field produced by hexagonal structure, which can be considered as perturbations and lead to the splitting of the $1S_{3/2}1S_e$ octet Efros et al. (1996), and the dielectric polarization effect owing the difference of the dielectric constant value between the NC material and TOPO, leading to a correction to the electron-hole Coulomb interaction Brus (1984). Thus, our approach provides a user-friendly tool to study different combinations of NC and surrounding materials and potential interesting physical effects, such as the crossover between strong and weak localization regimes for the QD hole.

5. Acknowledgements

The work was supported by the FCT (Portugal) under the grant PTDC/FIS/113199/2009. The authors are grateful to Prof. U. Woggon and Dr. O. Schï£¡ps for providing the photoluminescence measurement results presented in Fig. 6.

6. Appendix

Appendix I. Transfer matrix for a constant potential

Electrons

Let

$$\mathbf{z}(r) = \begin{pmatrix} \psi \\ \psi' \end{pmatrix} = \mathbf{M}(r) \cdot \mathbf{c}$$

where $\mathbf{c}$ is a 2-component constant vector, and

$$\mathbf{M}(r) = \begin{bmatrix} \cos(k_e r) & \sin(k_e r) \\ -k_e \sin(k_e r) & k_e \cos(k_e r) \end{bmatrix} \qquad (E_e > V_e)$$

or

$$\mathbf{M}(r) = \begin{bmatrix} \exp(\kappa_e r) & \exp(-\kappa_e r) \\ \kappa_e \exp(\kappa_e r) & -\kappa_e \exp(-\kappa_e r) \end{bmatrix} \qquad (E_e < V_e).$$

The key idea is to obtain $\mathbf{z}(r_2)$ given $\mathbf{z}(r_1)$:

$$\mathbf{z}(r_2) = \mathbf{T}(r_1, r_2) \cdot \mathbf{z}(r_1)$$

where $\mathbf{T}(r_1, r_2)$ is the transfer matrix. If r_1, r_2 are in the same material, the transfer matrix is $\mathbf{T}(r_1, r_2) = \mathbf{M}(r_2) \cdot \mathbf{M}^{-1}(r_1)$. Equivalently,

$$\mathbf{T}(r_1, r_2) = \begin{bmatrix} \cos(k_e \Delta r) & \frac{1}{k_e} \sin(k_e \Delta r) \\ -k_e \sin(k_e \Delta r) & \cos(k_e \Delta r) \end{bmatrix} \qquad (E_e > V_e)$$

or

$$\mathbf{T}(r_1, r_2) = \begin{bmatrix} \cosh(\kappa_e \Delta r) & \frac{1}{\kappa_e} \sinh(\kappa_e \Delta r) \\ \kappa_e \sinh(\kappa_e \Delta r) & \cosh(\kappa_e \Delta r) \end{bmatrix} \qquad (E_e < V_e).$$

At the interface Σ we have

$$\mathbf{z}(r^+) = \mathbf{T}_\Sigma \cdot \mathbf{z}(r^-),$$
$$\mathbf{T}_\Sigma = \begin{bmatrix} \beta_e^{-\alpha} & 0 \\ \frac{\beta_e^{-\alpha} - \beta_e^{\alpha+1}}{r} & \beta_e^{\alpha+1} \end{bmatrix},$$

and $\beta_e = m_e^+ / m_e^-$.

Holes

In this case

$$\mathbf{z}(r) = \begin{pmatrix} R_0 \\ R_2 \\ R_o' \\ R_2' \end{pmatrix} = \mathbf{M}(r) \cdot \mathbf{c}\,,$$

where $\mathbf{c}$ is a 4-component constant vector and

$$\mathbf{M}(r) = \begin{bmatrix} j_0(k_h r) & j_0(k_l r) & y_0(k_h r) & y_0(k_l r) \\ j_2(k_h r) & -j_2(k_l r) & y_2(k_h r) & -y_2(k_l r) \\ k_h j_0'(k_h r) & k_l j_0'(k_l r) & k_h y_0'(k_h r) & k_l y_0'(k_l r) \\ k_h j_2'(k_h r) & -k_l j_2'(k_l r) & k_h y_2'(k_h r) & -k_l y_2'(k_l r) \end{bmatrix} \qquad (E_h > V_h)$$

or

$$\mathbf{M}(r) = \begin{bmatrix} i_0(\kappa_h r) & i_0(\kappa_l r) & k_0(\kappa_h r) & k_0(\kappa_l r) \\ -i_2(\kappa_h r) & i_2(\kappa_l r) & -k_2(\kappa_h r) & k_2(\kappa_l r) \\ \kappa_h i_0'(\kappa_h r) & \kappa_l i_0'(\kappa_l r) & \kappa_h k_0'(\kappa_h r) & \kappa_l k_0'(\kappa_l r) \\ -\kappa_h i_2'(\kappa_h r) & \kappa_l i_2'(\kappa_l r) & -\kappa_h k_2'(\kappa_h r) & \kappa_l k_2'(\kappa_l r) \end{bmatrix} \qquad (E_h < V_h).$$

The transfer matrix is $\mathbf{T}(r_1, r_2) = \mathbf{M}(r_2) \cdot \mathbf{M}^{-1}(r_1)$.

At the interface (Σ) we have:

$$\mathbf{T}_{\Sigma} = \begin{bmatrix} 1 & 0 & 0 & 0 \\ 0 & 1 & 0 & 0 \\ 0 & 0 & \frac{1}{2}(\beta_l + \beta_h) & \frac{1}{2}(\beta_l - \beta_h) \\ 0 & 0 & \frac{1}{2}(\beta_l - \beta_h) & \frac{1}{2}(\beta_l + \beta_h) \end{bmatrix},$$

and $\beta_l = \frac{m_{lh}^{+}}{m_{lh}^{-}}$, $\beta_h = \frac{m_{hh}^{+}}{m_{hh}^{-}}$.

Appendix II. Numerical transfer matrix

The solution of the first-order ordinary differential equation,s

$$\hat{L}[\mathbf{z}(t)] = 0$$

$$\mathbf{z}(t_1) = \mathbf{a}$$

where $\hat{L}$ is a linear operator, $\mathbf{a} = (a_1, a_2, ..., a_n)$, and $\mathbf{z} : \Re \to \Re^n$, can be expressed in terms of the solution of the auxiliary problems:

$$\hat{L}[\mathbf{u}_i(t)] = 0$$

$$\mathbf{u}_i(t_1) = \mathbf{E}_i$$

where $\mathbf{E}_i \in \Re^n$ is the i-th canonical vector, and $i = 1, 2, ..., n$. Since

$$\mathbf{a} = \sum_{i=1}^{n} \mathbf{E}_i a_i,$$

we have

$$\mathbf{z} = \sum_{i=1}^{n} \mathbf{u}_i a_i,$$

in particular,

$$\mathbf{z}(t_2) = \sum_{i=1}^{n} \mathbf{u}_i(t_2) a_i.$$

Taking into account that $z_i(t_1) = a_i$, and denoting $T_{ji} = (u_i)_j$,

$$\mathbf{z}(t_2) = \mathbf{T} \cdot \mathbf{z}(t_1).$$

Hence the transfer matrix $\mathbf{T}$ is given by the solutions $\mathbf{u}_i$ putted as column vectors.

Appendix III. Infinite potential barrier in A_N

For electron, the condition is now $\varphi(A_N) = 0$, hence the equation

$$\mathbf{v}_3[1] = 0 \tag{18}$$

instead of (10) determinates the electron energy E_e. The constant c_1 can be obtained from normalization.

For holes, we have now $R_0(A_N) = R_2(A_N) = 0$, hence the equation

$$\begin{bmatrix} v_5[1] & v_6[1] \\ v_5[2] & v_6[2] \end{bmatrix} \cdot \begin{pmatrix} c_1 \\ c_2 \end{pmatrix} = \begin{pmatrix} 0 \\ 0 \end{pmatrix} \tag{19}$$

replaces (12) and E_h is given by

$$\det\left(\begin{bmatrix} v_5[1] & v_6[1] \\ v_5[2] & v_6[2] \end{bmatrix}\right) = 0. \tag{20}$$

7. References

Abramowitz, M. & Stegun, I. A. (1970). *Handbook of Mathematical Functions*.

Baccarani, G., Riccó, B. & Spadini, G. (1978). Transport properties of polycrystalline silicon films, *Journal of Applied Physics* 49(11): 5565.
URL: *http://link.aip.org/link/JAPIAU/v49/i11/p5565/s1&Agg=doi*

Baranov, A., Rakovich, Y., Donegan, J., Perova, T., Moore, R., Talapin, D., Rogach, a., Masumoto, Y. & Nabiev, I. (2003). Effect of ZnS shell thickness on the phonon spectra in CdSe quantum dots, *Physical Review B* 68(16): 1–7.
URL: *http://link.aps.org/doi/10.1103/PhysRevB.68.165306*

Bir, G. L. & Pikus, G. E. (1974). *Symmetry and Strain-Induced Effects in Semiconductors*, Wiley, New York.

Born, M. & Wolf, E. (1989). *Principles of Optics*, Pergamon, Oxford.

Brus, L. E. (1984). Electron-electron and electron-hole interactions in small semiconductor crystallites: The size dependence of the lowest excited electronic state, *The Journal of Chemical Physics* 80(9): 4403.
URL: *http://link.aip.org/link/JCPSA6/v80/i9/p4403/s1&Agg=doi*

Chen, O., Yang, Y., Wang, T., Wu, H., Niu, C., Yang, J. & Cao, Y. C. (2011). Surface-Functionalization-Dependent Optical Properties of II-VI Semiconductor Nanocrystals., *Journal of the American Chemical Society* 133(43): 17504–12.
URL: *http://www.ncbi.nlm.nih.gov/pubmed/21954890*

Dabbousi, B. O., Rodriguez-Viejo, J., Mikulec, F. V., Heine, J. R., Mattoussi, H., Ober, R., Jensen, K. F. & Bawendi, M. G. (1997). (CdSe)ZnS Core-Shell Quantum Dots: Synthesis and Characterization of a Size Series of Highly Luminescent Nanocrystallites, *The Journal of Physical Chemistry B* 101(46): 9463–9475.
URL: *http://pubs.acs.org/doi/abs/10.1021/jp971091y*

Delerue, C. & Lannoo, M. (2004). *Nanostructures. Theory and Modeling*, Springer-Verlag: Berlin.

Efros, A. L., Rosen, M., Kuno, M., Nirmal, M., Norris, D. J. & Bawendi, M. (1996). Band-edge exciton in quantum dots of semiconductors with a degenerate valence band: Dark and bright exciton states, *Phys. Rev. B* 54: 4843–4856.
URL: *http://link.aps.org/doi/10.1103/PhysRevB.54.4843*

Empedocles, S. A., Norris, D. J. & Bawendi, M. G. (1996). Photoluminescence spectroscopy of single cdse nanocrystallite quantum dots, *Phys. Rev. Lett.* 77: 3873–3876.
URL: *http://link.aps.org/doi/10.1103/PhysRevLett.77.3873*

Flory, C. C., Musgrave, C. C. & Zhang, Z. (2008). Quantum dot properties in the multiband envelope-function approximation using boundary conditions based upon first-principles quantum calculations, *Physical Review B* 77(20): 1–13.
URL: *http://prb.aps.org/abstract/PRB/v77/i20/e205312*

Fomin, V. M., Gladilin, V. N., Devreese, J. T., Pokatilov, E. P., Balaban, S. N. & Klimin, S. N. (1998). Photoluminescence of spherical quantum dots, *Phys. Rev. B* 57: 2415–2425.
URL: *http://link.aps.org/doi/10.1103/PhysRevB.57.2415*

Gaponik, N., Hickey, S. G., Dorfs, D., Rogach, A. L. & Eychmüller, A. (2010). Progress in the light emission of colloidal semiconductor nanocrystals., *Small (Weinheim an der*

Bergstrasse, Germany) 6(13): 1364–78.
URL: *http://www.ncbi.nlm.nih.gov/pubmed/20564480*

Gelmont, B. L. & Diakonov, M. I. (1972). *Sov. Phys. Semicond.* 5: 1905.

Grundmann, M., Christen, J., Ledentsov, N. N., Böhrer, J., Bimberg, D., Ruvimov, ‡, S. S., Werner, P., Richter, U., Gösele, U., Heydenreich, J., Ustinov, V. M., Egorov, A. Y., Zhukov, A. E., Kop'ev, P. S. & Alferov, Z. I. (1995). Ultranarrow luminescence lines from single quantum dots, *Phys. Rev. Lett.* 74: 4043–4046.
URL: *http://link.aps.org/doi/10.1103/PhysRevLett.74.4043*

Grundmann, M. (ed.) (2002). *Nano-Optoelectronics. Concepts, Physics and Devices*, Springer-Verlag, Berlin.

Hines, M. A. & Guyot-Sionnest, P. (1996). Synthesis and characterization of strongly luminescing zns-capped cdse nanocrystals, *The Journal of Physical Chemistry* 100(2): 468–471.
URL: *http://pubs.acs.org/doi/abs/10.1021/jp9530562*

Jasieniak, J., Califano, M. & Watkins, S. E. (2011). Size-dependent valence and conduction band-edge energies of semiconductor nanocrystals., *ACS nano* 5(7): 5888–902.
URL: *http://www.ncbi.nlm.nih.gov/pubmed/21662980*

Laikhtman, B. (1992). Boundary conditions for envelope functions in heterostructures, *Phys. Rev. B* 46: 4769–4774.
URL: *http://link.aps.org/doi/10.1103/PhysRevB.46.4769*

Larramendi, E. M. (n.d.). To be published.

Li, Y., Walsh, A., Chen, S., Yin, W., Yang, J., Li, J., Da Silva, J., Gong, X. & Wei, S. (2009). Revised ab initio natural band offsets of all group IV, II-VI, and III-V semiconductors, *Applied Physics Letters* 94: 212109.
URL: *http://link.aip.org/link/?APPLAB/94/212109/1*

Luo, X., Liu, P., Truong, N., Farva, U. & Park, C. (2011). Photoluminescence Blue-Shift of CdSe Nano-Particles Caused By Exchange of Surface Capping Layer, *The Journal of Physical Chemistry C* pp. 20817–20823.
URL: *http://dx.doi.org/10.1021/jp200701x*

Luttinger, J. M. (1956). Quantum theory of cyclotron resonance in semiconductors: General theory, *Phys. Rev.* 102: 1030–1041.
URL: *http://link.aps.org/doi/10.1103/PhysRev.102.1030*

Miranda, R. P., Vasilevskiy, M. I. & Trallero-Giner, C. (2006). Nonperturbative approach to the calculation of multiphonon raman scattering in semiconductor quantum dots: Polaron effect, *Phys. Rev. B* 74: 115317.
URL: *http://link.aps.org/doi/10.1103/PhysRevB.74.115317*

Murray, C., Norris, D. & Bawendi, M. (1993). Synthesis and characterization of nearly monodisperse CdE (E= S, Se, Te) semiconductor nanocrystallites, *Journal of American Chemical Society* 115(4): 8706–8715.
URL: *http://cat.inist.fr/?aModele=afficheN&cpsidt=18785986*

Norris, D. & Bawendi, M. G. (1996). Measurement and assignment of the size-dependent optical spectrum in CdSe quantum dots, *Physical Review B* 53(24): 16338.
URL: *http://prb.aps.org/abstract/PRB/v53/i24/p16338_1*

Pellegrini, G., Mattei, G. & Mazzoldi, P. (2005). Finite depth square well model: Applicability and limitations, *Journal of Applied Physics* 97(7): 073706.
URL: *http://link.aip.org/link/JAPIAU/v97/i7/p073706/s1&Agg=doi*

Rashad, M., Paluga, M., Pawlis, a., Lischka, K., Schikora, D., Artemyev, M. V. & Woggon, U. (2010). MBE overgrowth of ex-situ prepared CdSe colloidal nanocrystals, *Physica Status Solidi (C)* 7(6): 1523–1525.
URL: *http://doi.wiley.com/10.1002/pssc.200983272*

Rodina, A., Alekseev, A., Efros, A., Rosen, M. & Meyer, B. (2002). General boundary conditions for the envelope function in the multiband k·p model, *Physical Review B* 65(12): 1–12.
URL: *http://link.aps.org/doi/10.1103/PhysRevB.65.125302*

Rogach, A. L. (ed.) (2008). *Semiconductor Nanocrystal Quantum Dots*, Springer-Verlag, Wien.

Rolo, A. G., Vasilevskiy, M. I., Hamma, M. & Trallero-Giner, C. (2008). Anomalous first-order raman scattering in iii-v quantum dots: Optical deformation potential interaction, *Phys. Rev. B* 78: 081304.
URL: *http://link.aps.org/doi/10.1103/PhysRevB.78.081304*

Schulz, S. & Czycholl, G. (2005). Tight-binding model for semiconductor nanostructures, *Phys. Rev. B* 72: 165317.
URL: *http://link.aps.org/doi/10.1103/PhysRevB.72.165317*

Soni, U. (2010). The Importance of Surface in Core-Shell Semiconductor Nanocrystals, *The Journal of Physical Chemistry C* 114: 22514.
URL: *http://pubs.acs.org/doi/abs/10.1021/jp1091637*

Springer Materials The Landolt-Börnstein Database (2011). Springer.

Talapin, D., Rogach, A., Kornowski, A., Haase, M. & Weller, H. (2001). Highly luminescent monodisperse CdSe and CdSe/ZnS nanocrystals synthesized in a hexadecylamine-trioctylphosphine oxide-trioctylphospine mixture, *Nano Letters* 1(4): 207–211.
URL: *http://pubs.acs.org/doi/abs/10.1021/nl0155126*

Vasilevskii, M., Akinkina, E., De Paula, A. & Anda, E. (1998). Effect of size dispersion on the optical absorption of an ensemble of semiconductor quantum dots, *Semiconductors* 32(11): 1229–1233.
URL: *http://www.springerlink.com/index/XW2V65248T002873.pdf*

Wang, X., Zhuang, J., Peng, Q. & Li, Y. (2005). A general strategy for nanocrystal synthesis, *Nature* 437(7055): 121–124.
URL: *http://www.nature.com/nature/journal/v437/n7055/suppinfo/nature03968_S1.html*

Woggon, U., Herz, E., Schöps, O., Artemyev, M. V., Arens, C., Rousseau, N., Schikora, D., Lischka, K., Litvinov, D. & Gerthsen, D. (2005). Hybrid epitaxial-colloidal semiconductor nanostructures., *Nano letters* 5(3): 483–90.
URL: *http://www.ncbi.nlm.nih.gov/pubmed/15755099*

Yu, W. W., Qu, L., Guo, W. & Peng, X. (2003). Experimental Determination of the Extinction Coefficient of CdTe, CdSe, and CdS Nanocrystals, *Chemistry of Materials* 15(14): 2854–2860.
URL: *http://pubs.acs.org/doi/abs/10.1021/cm034081k*